PHOTONICS Research

Bifunctional ultraviolet light-emitting/detecting device based on a SnO_2 microwire/p-GaN heterojunction

TONG XU,[1] MINGMING JIANG,[1,*] PENG WAN,[1] KAI TANG,[1] DANING SHI,[1] AND CAIXIA KAN[1,2]

[1]College of Science, MIIT Key Laboratory of Aerospace Information Materials and Physics, Key Laboratory for Intelligent Nano Materials and Devices, Nanjing University of Aeronautics and Astronautics, Nanjing 211106, China

[2]e-mail: cxkan@nuaa.edu.cn

*Corresponding author: mmjiang@nuaa.edu.cn

Received 31 August 2021; revised 7 October 2021; accepted 18 October 2021; posted 19 October 2021 (Doc. ID 441999); published 19 November 2021

SnO_2 has attracted considerable attention due to its wide bandgap, large exciton binding energy, and outstanding electrical and optoelectronic features. Owing to the lack of reliable and reproducible p-type SnO_2, many challenges on developing SnO_2-based optoelectronic devices and their practical applications still remain. Herein, single-crystal SnO_2 microwires (MWs) are acquired via the self-catalyzed approach. As a strategic alternative, n-SnO_2 MW/p-GaN heterojunction was constructed, which exhibited selectable dual-functionalities of light-emitting and photodetection when operated by applying an appropriate voltage. The device illustrated a distinct near-ultraviolet light-emission peaking at ~395.0 nm and a linewidth ~50 nm. Significantly, the device characteristics, in terms of the main peak positions and linewidth, are nearly invariant as functions of various injection current, suggesting that quantum-confined Stark effect is essentially absent. Meanwhile, the identical n-SnO_2 MW/p-GaN heterojunction can also achieve photovoltaic-type light detection. The device can steadily feature ultraviolet photodetecting ability, including the ultraviolet/visible rejection ratio ($R_{360\,nm}/R_{400\,nm}$) ~1.5×10^3, high photodark current ratio of 10^5, fast response speed of 9.2/51 ms, maximum responsivity of 1.5 A/W, and detectivity of 1.3×10^{13} Jones under 360 nm light at −3 V bias. Therefore, the bifunctional device not only displays distinct near-ultraviolet light emission, but also has the ability of high-sensitive ultraviolet photodetection. The novel design of n-SnO_2 MW/p-GaN heterojunction bifunctional systems is expected to open doors to practical application of SnO_2 microstructures/nanostructures for large-scale device miniaturization, integration and multifunction in next-generation high-performance photoelectronic devices. © 2021 Chinese Laser Press

https://doi.org/10.1364/PRJ.441999

1. INTRODUCTION

Fabrication of multifunctional optoelectronic devices, especially for the low-dimensional devices, has regarded as the rising demand of energy conservation, miniaturization, high-integration, being portable in many daily life aspects [1–8]. Because of its wide bandgap and a high exciton-binding energy (~3.62 eV, ~130 meV at room temperature), high quantum efficiency, stability and high electron mobility, tin dioxide (SnO_2) is frequently used as a potential candidate to develop many practical devices, such as gas sensors, transparent conductors, photodetectors, light-emitting devices, and solar cells [9–15]. Owing to its natural n-type conductivity, it is still a serious bottleneck to prepare stable and reproducible p-type SnO_2. Alternatively, the p-GaN film layer has been commonly utilized to fabricate SnO_2-based heterojunction optoelectronic devices, due to the wide application and mature doping technology [2,14,16–18]. Nevertheless, being restricted to the dipole-forbidden and intrinsic defects including Sn interstitials, dangling bonds, or oxygen vacancies, the vast majority of the previously reported works have illustrated that bulk SnO_2-based emission devices mostly emit broad luminescence at the visible wavelengths, instead of ultraviolet light emission [15,19]. Lately, low dielectric layers, such as MgO and AlN, have been introduced into SnO_2/GaN-based heterojunction LEDs to improve the device performance. In addition, low-dimensional SnO_2, including quantum dots, nanowire, nanotubes, nanowire arrays, microwire/rods, and so on, has been prepared to construct ultraviolet light sources, and eventually used to break through the dilemma of the "forbidden" bandgap due to large surface-to-volume ratios, low cost, strong radiation hardness, and high chemical stability [14,16,17,20].

As a typical wide-bandgap semiconductor, SnO_2 has attracted great attention in the field of fabricating ultraviolet photodetection devices [8,21–26]. Based on the photoelectric effect, SnO_2-based structures and devices can transform optical information into electrical signals, providing a competitive candidate to develop ultraviolet photodetecting devices. Numerous studies reported that SnO_2 thin film, nanowire, nanonet, nanofiber, nanobelt, and microrod/wires have been utilized to fabricate ultraviolet photodetectors with their applications in missile early warning, flame sensing, environmental monitoring, and wireless communications [2,27–31]. Many groups have presented that SnO_2 nanowires have been extensively used to construct high-performance ultraviolet photodetectors [12,13,32–34]. For instance, Chen *et al.* fabricated SnO_2–NiO heterojunction nanonets, exhibiting a high ultraviolet detectivity [35]; and Tian *et al.* reported ZnO–SnO_2 heterojunction nanofibers, yielding a high photocurrent in ultraviolet region [32,36–38]. However, the device performances, including the dark current and response time of the works mentioned above, are still dissatisfactory [18,39,40]. There remains a lot of work to do to improve the response time and photocurrent while reducing the dark current of the as-constructed SnO_2-based photodetecting devices [31,41–46].

To satisfy some special requirements in practical applications with regard to excellent electroluminescent and photovoltaic properties, studies on the synthesis of low-dimensional semiconductors and the construction of optoelectronic devices with bifunctional electronics are particularly important [5,47–50]. In this work, individual SnO_2 microwires (MWs) with high crystallinity and well-defined geometries have been prepared utilizing a facile vapor transport deposition (CVD) method. Employing p-type GaN as the hole transporting layer, we demonstrate an ultraviolet light emission and detection dual-functioning device based on a single SnO_2 MW upon the operation of both forward and reverse biasing conditions, respectively. As the forward bias beyond the turn-on voltage, the fabricated n-SnO_2 MW/p-GaN heterojunction device exhibits significant near-ultraviolet electroluminescence (EL) with a pronounced peak luminescence at 395.0 nm, and the spectral linewidth is extracted to about 50 nm. Simultaneously, the heterojunction also demonstrates excellent ultraviolet photodetecting features, containing a large responsivity of 1.5 A/W, a detectivity of 1.3×10^{13} Jones, a high external quantum efficiency (EQE) of 497%, a large photo-to-dark current (I_{on}/I_{off}) ratio of 10^5, an ultraviolet/visible rejection ratio of about 1.5×10^3, and a fast response speed of 9.2/51 ms under 360 nm light at a reverse bias of −3.0 V. These experimental results exhibit that the simple and easy fabrication of n-SnO_2 MW/p-GaN heterojunction provides a new and promising scheme for developing ultraviolet bifunctional optoelectronic devices, as well as for practical applications.

2. EXPERIMENTAL SECTION

A. Synthesis of Individual SnO_2 MWs

Single-crystal SnO_2 MWs were prepared utilizing a simple CVD method [24,29,30]. In the process of preparing microstructured SnO_2, a high-temperature tube furnace is used as the crystal growth equipment. A mixture of high-purity powders of SnO_2 and graphite (C) (the weight ratio of 1:1) was put in a corundum boat. A cleaned Si wafer was placed on a corundum boat to collect the samples. The growth procedure was summarized as follows: (1) to guarantee that tube furnace was an oxygen-deficient environment, a constant flow of argon (Ar) (99.99%) (125 sccm) was first introduced into the tube furnace; (2) the corundum boat was put into a quartz tube, and the precursor mixture was placed at the hottest zone; (3) the temperature was raised to 1100°C at a rate of 20°C per minute, and served as growth temperature; (4) with the oxygen-deficient composited condition maintained for ∼1 h, 10% oxygen (O_2) was introduced into the furnace chamber as the growth gas for about 30 min; (5) the furnace chamber was then naturally cooled to room temperature. SnO_2 product can be collected around the Si wafer. The diameter of the wires varies in the region of 0.5–20 μm, and their length can reach up to 1 cm. By optimizing the growth condition including the growth temperature, and the carrier gas, SnO_2 MWs with higher crystallization quality can be improved.

B. Fabrication of n-SnO_2 MW/p-GaN Heterojunction

A heterostructured device made of an individual n-SnO_2 MW and p-type GaN substrate was prepared. In the heterostructure, commercially purchased p-type GaN substrate was utilized as the hole transporting layer. The device preparation is summarized as follows: (1) Ni/Au films with the thickness of 30/40 nm were first prepared on an activated p-type GaN layer; (2) MgO insulating films (∼100 nm in thickness) were deposited on one side of the GaN film utilizing electron beam heating evaporation; (3) a single SnO_2 MW with the diameter of about 10 μm was subsequently placed across the p-GaN film and MgO layer, and an In particle was fixed on the wire on the MgO layer; thus, the MgO layer serving as an insulating layer was utilized to prevent the direct contacting between the In electrode and the p-GaN substrate. In the device structure, In and Ni/Au were employed as electrodes for the current injection. The device configuration is schematically depicted later in the paper [51,52].

3. RESULTS AND DISCUSSION

A. n-SnO_2 MW/p-GaN Heterojunction LED

As we described in the experimental section, individual SnO_2 MWs with well-defined geometries, specifically for the quadrilateral cross section, were successfully prepared [24,29,30]. The optical picture of as-grown MWs is shown in Fig. 1(a). A scanning electron microscopy (SEM) image of SnO_2 MWs is displayed in Fig. 1(b). It illustrates that the average diameter of the as-synthesized MWs is approximately about 5 μm. In addition, a quadrilateral cross section can also be observed in Fig. 1(c). The elemental mapping of an individual SnO_2 MW was determined by energy-dispersive X-ray spectroscopy (EDS). As shown in Figs. 1(d)–1(f), the elements of Sn and O are uniformly distributed throughout a single wire. Typical transmission electron microscopy (TEM) images of an individual SnO_2 wire (the diameter ∼500 nm) with a straight boundary were examined, and its high-resolution TEM picture is displayed in Fig. 1(g). From the figure, the wire demonstrates clear lattice

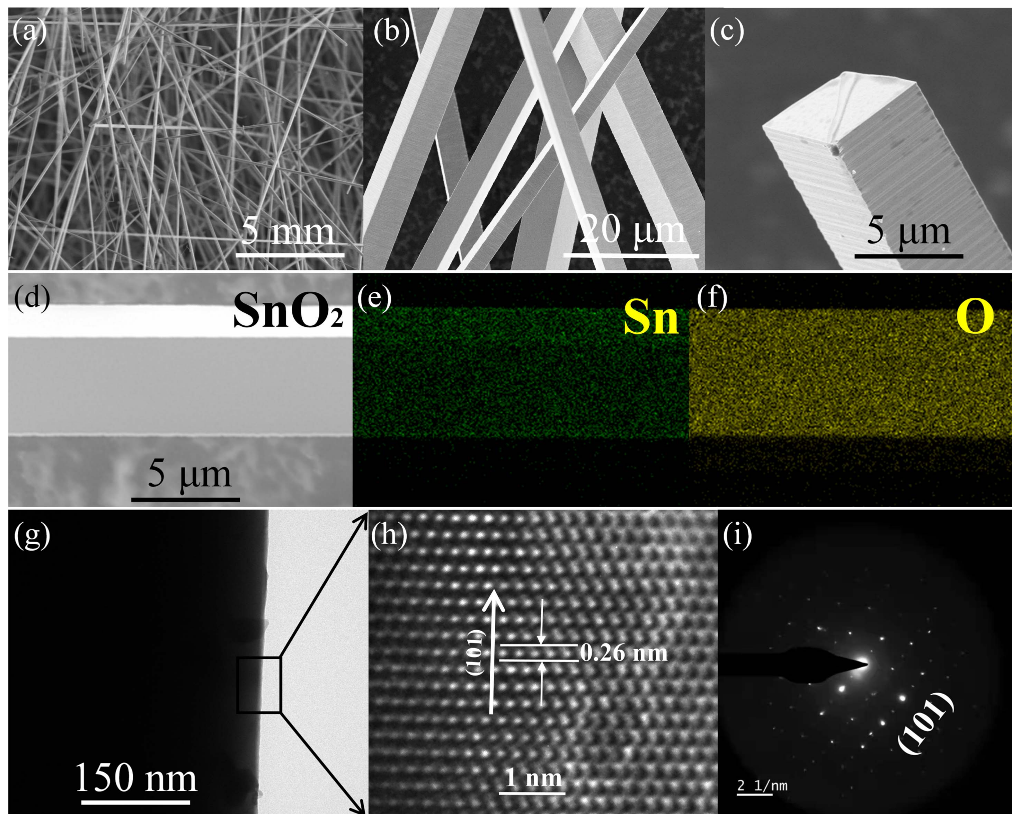

Fig. 1. Characterization of the prepared SnO_2 MWs. (a) Optical photograph of individual SnO_2 MWs. (b) Enlarged SEM image of several SnO_2 MWs. (c) Quadrilateral cross section of an individual SnO_2 MW. (d)–(f) EDS elemental mapping results of Sn and O species from a selected MW. (g) Lower-resolution TEM picture of a single SnO_2 wire, the diameter was measured to about 500 nm. (h) Corresponding high-resolution TEM image marked in (g). (i) SAED image of a SnO_2 wire. It suggests that the as-grown SnO_2 wires are preferentially exposing (101) orientation.

fringes, and the interplanar space is extracted to be about 0.260 nm [30,31]. Further, the single-crystalline character of the as-synthesized SnO_2 wire was featured by using the electron diffraction (SAED) pattern, which corresponded to the (101) plane of rutile SnO_2 [see Fig. 1(i)]. Therefore, the as-synthesized SnO_2 MWs were well-crystallized in the single-crystal rutile structure [35,41].

The illustration in Fig. 2(a) is a schematic of a heterojunction LED, which is made of a SnO_2 MW and p-type GaN substrate. In the device configuration, the p-type GaN substrate serves as the hole transporting layer [2,14]. To study the device performance, the electrical contacting character of the n-SnO_2 MW/p-GaN heterojunction was first measured by using a Keysight semiconductor device analyzer (B1500A). The current-voltage (I-V) curve is plotted in Fig. 2(b), indicating that the curve illustrates a well-defined diode-like rectifying behavior. To investigate the electrical behavior, the electronic transport properties of an individual SnO_2 MW were examined, and the I-V curve is illustrated in the inset of Fig. 2(b) (in the electrical measurement, In particles serve as the electrodes). The plotted curve illustrates linear behavior, confirming that the In electrode makes a good ohmic contact with the SnO_2 MW. Ni/Au was evaporated on the p-GaN template utilizing the electron-beam evaporation system. Afterwards, an annealing treatment was further implemented in air. An I-V curve shown in the inset of Fig. 2(b) displays a linear feature, and thus, ohmic contact behavior was formed between the Ni/Au and p-GaN substrate (the red solid line) [7,53]. The diode-like rectification characteristic is attributed to the high-quality heterojunction formed between the n-SnO_2 MW and p-GaN substrate. Specifically, the device has a turn-on voltage of ~4.0 V, and a negligibly small leakage current, which was evaluated to $\sim 3.9 \times 10^{-11}$ A even at −5 V bias. Therefore, an n-SnO_2 MW/p-GaN heterojunction can be utilized to construct a one-dimensional wired optoelectronic device.

Varying the forward bias above the turn-on voltage, the electrically driven luminescence from the as-fabricated n-SnO_2 MW/p-GaN heterojunction LED was tested by utilizing the PIXIS 1024BR CCD detection system at room temperature. Figure 2(c) displays the collected EL spectra. It represents a dominant near-ultraviolet emission with a main peak wavelength of about 395.0 nm. Noticeably, the main peak wavelengths keep an almost constant value by increasing the injection current, while the spectral linewidths of the EL spectra are checked to about 50 nm, and the linewidths are nearly invariant with various input currents. Compared with conventional GaN-based ultraviolet light emitters which severely suffer from quantum-confined Stark effect, the fabricated n-SnO_2 MW/p-GaN heterojunction LEDs exhibit extraordinary stability. Figure 2(d) plots the driving current-dependent integrated

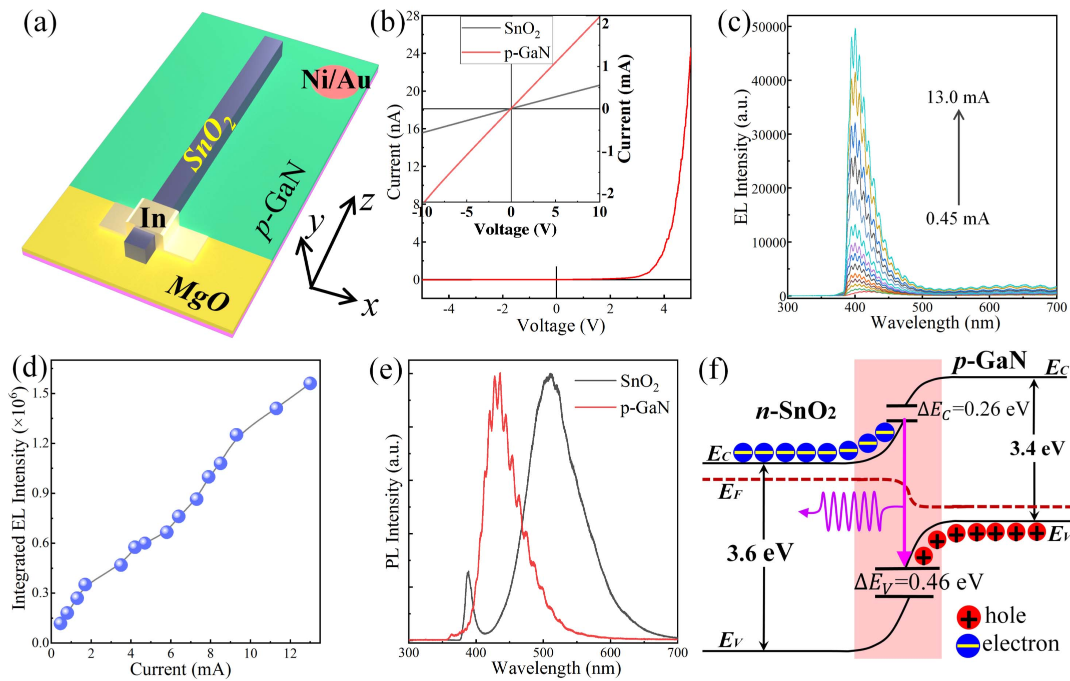

Fig. 2. Characterization of the fabricated n-SnO_2 MW/p-GaN heterojunction LED. (a) Straightforward illustration of a near-ultraviolet LED structure, which is made of an individual SnO_2 MW and p-GaN substrate. In the device architecture, In and Ni/Au are employed as electrodes for the current injection. (b) *I-V* curve of the fabricated SnO_2 MW/p-GaN heterostructure, suggesting diode-like rectifying characteristic. Inset: *I-V* curves of an individual SnO_2 MW and p-type GaN template, yielding ohmic contact behaviors. (c) The EL spectra as a function of the input current varied from 0.45 to 13.0 mA. (d) Variation of integrated EL intensity versus injection current. (e) Normalized PL spectra of a SnO_2 MW and p-type GaN substrate, respectively. (f) Schematic of the energy band diagram of n-SnO_2 MW/p-GaN heterojunction.

EL intensity, showing nearly linear characteristics. The linear rise of integrated EL intensity with regard to the input current indicates a very small Shockley–Read–Hall recombination coefficient in the SnO_2 MW LED. Therefore, the well-formed one-dimensional wired n-SnO_2/p-GaN heterojunction can be ascribed to the dramatically lower defects and negligible nonradiative recombination at the surfaces of SnO_2 nanostructures/microstructures [2,16,17].

To exploit the near-ultraviolet EL features of the as-fabricated n-SnO_2 MW/p-GaN heterojunction LED, optical characterization of a SnO_2 MW and GaN template was performed by using He–Cd laser at an excitation wavelength of 325 nm. The photoluminescence (PL) spectra were collected by utilizing a spectrometer via an Andor Newton electron multiplying CCD camera (Horiba Jobin-Yvon iHR500). The PL spectrum of a SnO_2 MW illustration in Fig. 2(e) (the black solid line) demonstrates that ultraviolet emission peaking at 380.0 nm was obtained, accompanied with a much stronger broadband emission in the visible band (the peak position locates at 510 nm). By optimizing the CVD method, the near-band-edge related PL can be acquired in the ultraviolet region due to the breakthrough of dipole forbidden rule. The broader and stronger light emission in the visible region is assigned to the radiative recombination, which is connected with the deep-level defects. It suggests that the as-grown SnO_2 MWs possess relative high crystal quality [2,14]. The optical characterization of the p-type GaN substrate was also performed by utilizing a He–Cd laser as an excitation laser source. Figure 2(e) displays the PL spectrum (the red solid line), illustrating that the main PL wavelength positions at around 435.5 nm, and the spectral linewidth is measured to be 50 nm. Accordingly, the EL peak energy of the device cannot be matched well with the near-band energy, or the deep-level energy of the SnO_2 MW; meanwhile, the near-ultraviolet EL cannot be matched with light radiation from direct band-to-band transition of the GaN film. Therefore, the EL results could be attributed to the radiative recombination at the n-SnO_2/p-GaN interface [2,14,17].

Compared with PL results of the SnO_2 MW and GaN layer, it is concluded that the near-ultraviolet EL of the fabricated LED cannot be simply derived from either the SnO_2 MW or the p-GaN substrate. The origin of the near-ultraviolet EL was examined. According to the electron affinities of SnO_2 (~4.50 eV) and GaN (~4.20 eV), a Type II energy band structure can be created at the n-SnO_2/p-GaN heterostructure, as depicted in Fig. 2(f) [2,30,45]. As the hole concentration in the p-type GaN template $\sim 10^{17}$ is much approximate to the electron concentration in the n-SnO_2 MW, thus, a formation of wider depletion region in the SnO_2 MW could be yielded. It is inferred that a conduction-band offset of ΔE_c is evaluated to be 0.26 eV, while the valence band offset of ΔE_v is evaluated to about 0.46 eV, producing a band discontinuity at the SnO_2/GaN interface. Owing to the much smaller band offset ($\Delta E_c \sim 0.26$ eV, $\Delta E_v \sim 0.46$ eV), electrons in the SnO_2 MW can leak into the p-type GaN layer, while the injected holes into the fabricated heterojunction device can leak from the p-type GaN layer into the n-SnO_2 MW. The obtained EL may be composed of the light emitting from the SnO_2

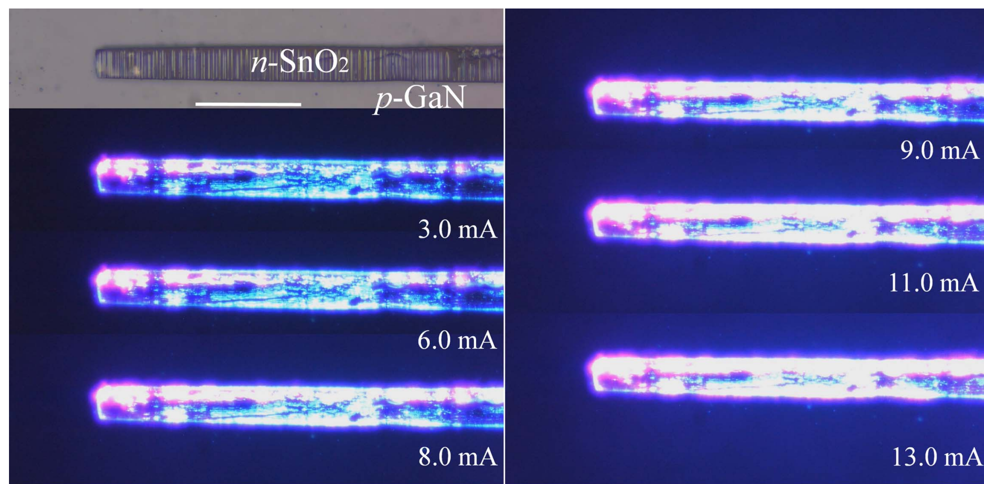

Fig. 3. When illuminated electrically at forward biasing condition, optical microscopic EL pictures of the as-fabricated n-SnO_2 MW/p-GaN LED were captured using a CCD, with the input current varied in the range of 3.0–13.0 mA. The scale bar is 25 μm.

MW, GaN layer, and the SnO_2/GaN interface. In particular, the ΔE_v is considerably larger than ΔE_c, and it can be figured out that electron injection from the n-SnO_2 MW into the p-GaN layer is much more advantageous by comparing with the hole injection. Consequently, efficient radiative recombinations of carriers are principally happening at the SnO_2/GaN interface, explaining the origin of near-ultraviolet EL upon the electrical excitation [2,14,17].

The near-ultraviolet emission characteristics of one-dimensional wired LED were studied by using a high numerical aperture microscope objective via a CCD camera (Olympus). Varying the injection current in the range of 3.0–13.0 mA, the optical microscopic EL images of blue–violet illuminating were captured, as shown in Fig. 3. From the figure, the near-ultraviolet light is mainly emitted out along both the lateral edges of the quadrilateral MW, and the EL intensity is periodically distributed around the quadrilateral microresonator. For the first time, the n-SnO_2 MW/p-GaN heterojunction emitting at ~395.0 nm is designed. The success of an individual SnO_2 MW with good crystal quality in designing ultraviolet LEDs paves the way toward practical applications of SnO_2 microstructure/nanostructure-based light sources. In addition, several light-emission devices on account of the n-SnO_2 MW/p-GaN heterojunction architecture were also constructed, as we described in Section 2. It is evidenced that the one-dimensional wired n-SnO_2/p-GaN heterojunction can be utilized to construct low-dimensional near-ultraviolet light sources. The fabricated LEDs demonstrated excellent stability and reproducibility, which are understandable due to the outstanding durability of well-crystallized SnO_2 MWs.

B. n-SnO_2 MW/p-GaN Heterojunction Photodetector

As we described above, the fabricated n-SnO_2 MW/p-GaN heterojunction also shows good LED-like characteristics with a negligible leakage current. Due to the much lower dark current, the n-SnO_2 MW/p-GaN heterojunction for fabricating high-performance photodetectors, which work at the ultraviolet wavelengths, was further examined. To this regard, the n-SnO_2 MW/p-GaN heterojunction feature as an ultraviolet photodetector was successfully demonstrated. A typical device configuration is shown in Fig. 4(a). In the device configuration, Ni/Au film deposited on the p-GaN film is employed as the cathode; while the In particle fixed on one end of the MW serves as the anode [2,29,30,54]. The electrical properties of the prepared photodetector under dark and ultraviolet radiation were tested at room temperature. As seen in Fig. 4(b), the I-V curve measured in the dark exhibits excellent rectification characteristics [blue solid line; also see Fig. 2(b)]. At 5 V bias, the current is about 2.5×10^{-8} A, while the reverse leakage current at −5 V is less than 3.9×10^{-11} A. Furthermore, the rectification ratio of the device was 6.5×10^2 at the biases of ±5 V. When exposed under the radiation of 360 nm light, the nonlinear I-V curve (red solid line) of the heterojunction photodetector represents an observable photoresponse. It shows an off-state current (less than 1.5×10^{-6} A) at the reverse bias and an on-state current (approaching 1.9×10^{-5} A) at the forward bias, suggesting a traditional p-n diode behavior.

When illuminated upon different light wavelengths, typical I-V curves of the device in a logarithmic plot are illustrated in Fig. 4(c) in the dark and differently illuminated lights of 300 nm (1.4 mW/cm^2), 320 nm (2.0 mW/cm^2), 340 nm (2.7 mW/cm^2), 360 nm (3.2 mW/cm^2), 380 nm (3.6 mW/cm^2), and 400 nm (4.4 mW/cm^2) by using a Xe lamp as light source. Shown in the figure, the fabricated n-SnO_2 MW/p-GaN photodetector displays differences in the photocurrent and dark current. It indicates that the fabricated device obtains significant ultraviolet photoelectric characters. The photocurrents of the prepared device could reach 3.4×10^{-5} at −5 V bias under 360 nm illumination, which is around 10^5 times of magnitude higher than that of the dark current. The photocurrent was lower under the illumination of 400 nm light but still kept at 2.1×10^{-9} A. The ultralow dark current and super-high photocurrent indicate that the single SnO_2 MW photodetector has a high signal-to-noise ratio. When the irradiated light wavelengths increase from 300 to 360 nm, the photocurrent increases gradually, which is due to the additional carrier generated by the incident light, as well as an increase of the optical power density. When the irradiated

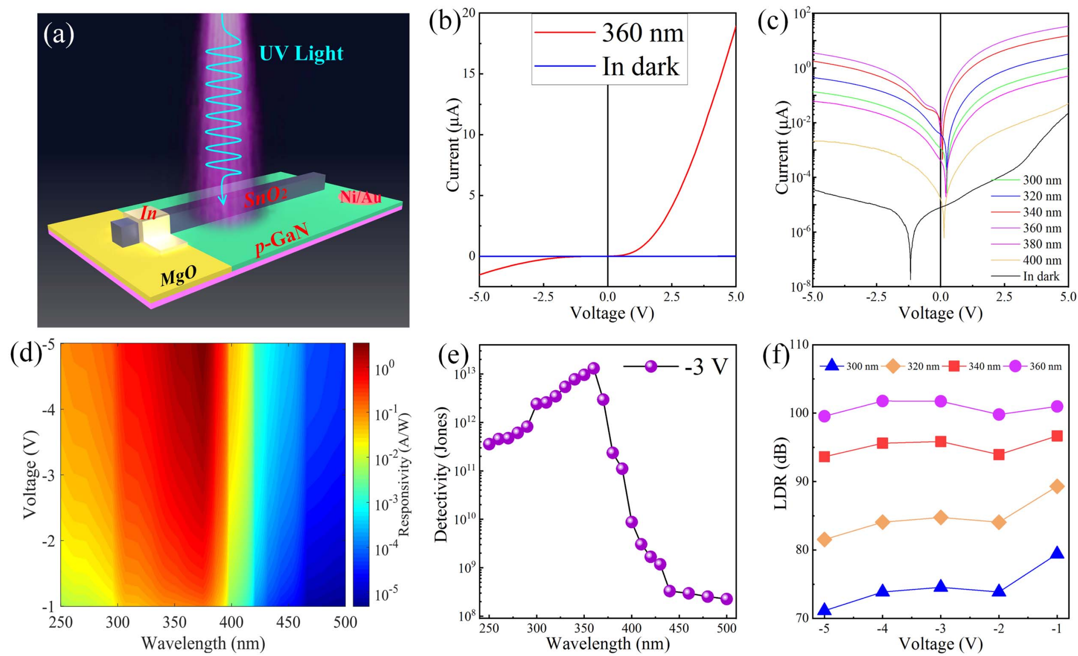

Fig. 4. Characterization of ultraviolet photodetecting features of the prepared n-SnO_2 MW/p-GaN heterojunction device. (a) Schematic diagram of the n-SnO_2 MW/p-GaN heterojunction photodetecting device. (b) The comparison of photocurrent on the fabricated n-SnO_2 MW/p-GaN heterojunction device under 360 nm light (upper, red) and dark (lower, blue). (c) I-V curves of the fabricated n-SnO_2 MW/p-GaN heterojunction photodetection apparatus under the dark, and illumination at different wavelengths in the ultraviolet regions. (d) Contour plot of the responsivity R of the as-prepared n-SnO_2 MW/p-GaN heterojunction photodetection apparatus as a function of light wavelengths of the ultraviolet illumination, and different bias. (e) The detectivity of as-fabricated n-SnO_2 MW/p-GaN heterojunction photodetection device as a function of wavelength at −3.0 V bias. (f) By varying the applied bias voltage in the region of −5.0 to −1.0 V, comparison of LDR spectra of as-prepared photodetectors when operated at different incident wavelengths.

wavelength is further increased to 380 and 400 nm, the photocurrent begins to decrease gradually because the bandgap of the active layers is larger than the incident photon energy.

To research the light wavelength selectivity of the as-fabricated n-SnO_2 MW/p-GaN photodetector, the corresponding response spectra were measured. The responsivity (R), one important performance metric of the photodetector, is first introduced. The parameter R is calculated as follows [24,55,56]:

$$R = \frac{I_P - I_D}{PS}. \tag{1}$$

In the formula, I_P, I_D, P, and S are the photocurrent, dark current, incident optical power, and effective irradiation area, respectively. The study of the ultraviolet photodetecting behavior in terms of the illumination wavelength and applied bias for the n-SnO_2 MW/p-GaN heterojunction photodetector was implemented. We calculated their photoresponse spectra. As seen in Fig. 4(d), the photodetector shows obvious response at the ultraviolet wavelength, and the photoresponse reaches its maximum value at about 360 nm. Thus, the single MW heterojunction photodetector has a representative photoresponse spectrum at the ultraviolet wavelengths. The spectral responsivities are primarily generated due to the absorption properties of the as-grown microstructured SnO_2. By calculation, the ultraviolet/visible rejection ratio ($R_{360\,\mathrm{nm}}/R_{400\,\mathrm{nm}}$) of the heterojunction photodetector is evaluated to be 1.5×10^3, indicating a prominent ultraviolet peculiarity of the photodetector. It is deduced that, increasing the reverse voltage of the device, significantly increased R can be achieved. At −1.0 V bias, the maximum responsivity R is extracted to about 0.13 A/W. Increasing the reverse voltage to be −3.0 V, the maximum responsivity R is evaluated to 1.5 A/W. As the reverse voltage increased up to −5.0 V, the maximum responsivity R is increased up to 3.5 A/W.

To assess the device performance of the presented n-SnO_2 MW/p-GaN heterojunction photodetector, the specific detectivity (D^*), another significant parameter of photodetectors, which shows the photodetector ability to capture very weak signals, can be expressed by the equation [41,57,58]

$$D^* = \frac{R\sqrt{A}}{\sqrt{2eI_D}}, \tag{2}$$

where R is the responsivity, A is the effective irradiation area, e is the electron charge, and I_d is the dark current. Due to Eq. (2), the detectivity D^* of the individual SnO_2 MW-based photodetector as a function of the illumination wavelength was calculated. As illustrated in Fig. 4(e), the maximum D^* is evaluated as high as 1.3×10^{13} Jones ($1\ \mathrm{Jones} = 1\ \mathrm{cm} \cdot \mathrm{Hz}^{1/2} \cdot \mathrm{W}^{-1}$) under 360 nm light. The detectivity is much higher than that of commercial Si and InGaAs photodetectors [8,24,27]. Further, the detectivity D^* of the fabricated n-SnO_2 MW/p-GaN heterojunction photodetector is also comparable to other high-performance ultraviolet photodetection devices [2,29,30,32].

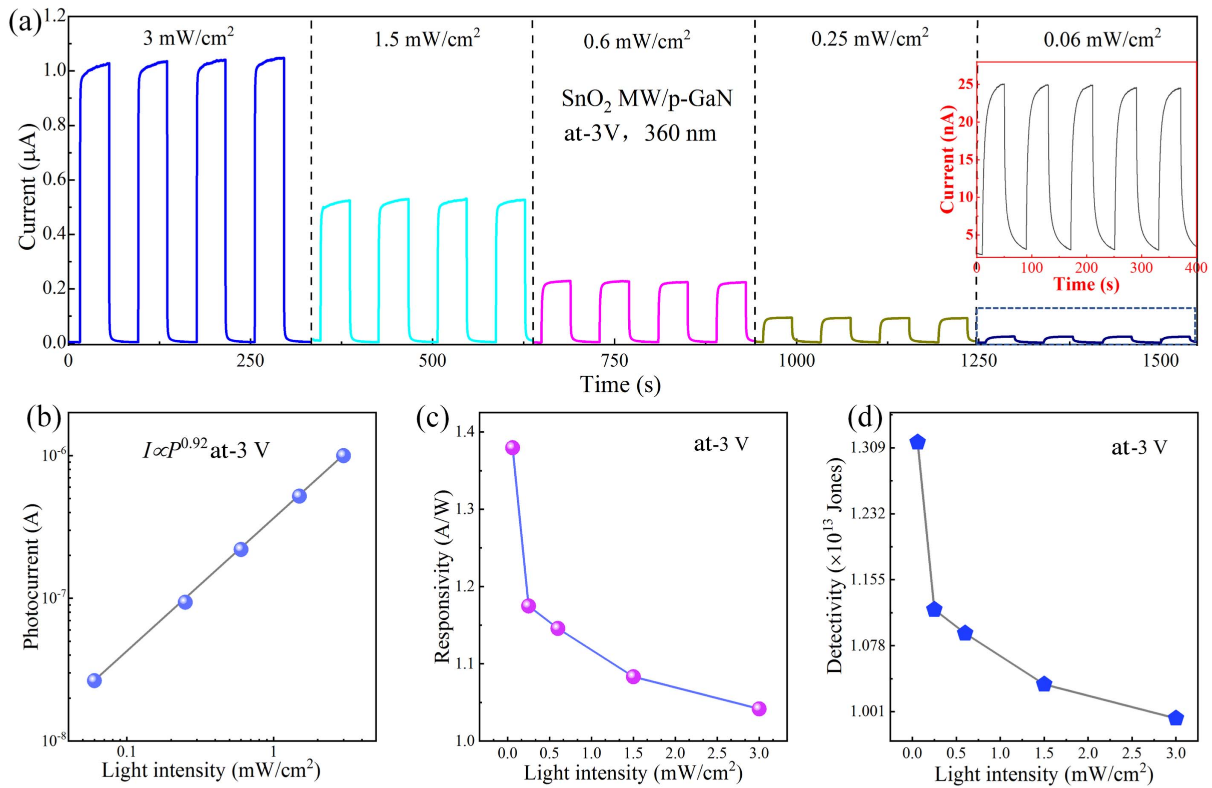

Fig. 5. (a) Light power-dependent photoresponse under ultraviolet illumination at the time scale. The device was illuminated at the light wavelength of 360 nm, and measured at a reverse bias of −3.0 V. Inset: the enlarged portions of I-t curve of the device from the highlighted part in (a), which operated upon the ultraviolet light illumination at the wavelength of 360 nm. (b) Logarithmic plot of the photocurrent versus incident light irradiation power at a reverse bias of −3.0 V. (c) Responsivity and (d) detectivity of the as-constructed n-SnO_2 MW/p-GaN heterojunction photodetector in terms of light intensity at −3 V bias.

The linear dynamic range (LDR) of the n-SnO_2 MW/p-GaN heterojunction device operated at various light wavelengths of ultraviolet illumination, was described by the following formula:

$$\mathrm{LDR} = 20\ \log(I_P/I_D). \quad (3)$$

In the formula, I_D is the dark current, and I_P is the photocurrent obtained at the illumination of ultraviolet light. As shown in Fig. 4(f), the LDR is obtained to be ∼100 dB at 360 nm, and this value is much larger than that of commercial photodetectors (∼66 dB). Additionally, the superhigh LDR (over 70 dB at the wavelengths of 300–360 nm) shows that the as-constructed n-SnO_2 MW/p-GaN heterojunction photodetector possesses a relatively large ratio of photocurrent to dark current, and has an extremely high signal-to-noise ratio. The results display that the fabricated n-SnO_2 MW/p-GaN heterojunction photodetector has excellent ultraviolet photodetecting features [2,59].

The photosensitivity of the n-SnO_2 MW/p-GaN heterojunction device was also tested at −3 V bias. Figure 5(a) displays the I-t characteristics of the photodetector under the 360 nm light utilizing irradiance with light power intensities varied in the range of 0.06–3.0 $\mathrm{mW/cm^2}$. By varying the light intensities, photocurrent responses increased steadily for the device. When the optical density is increased from 0.06 to 3.0 $\mathrm{mW/cm^2}$, the photoresponse of the photodetector aggrandizes with photocurrent values of 2.86 nA at 0.06 $\mathrm{mW/cm^2}$, 95 nA at 0.25 $\mathrm{mW/cm^2}$, 230 nA at 0.60 $\mathrm{mW/cm^2}$, and 500 nA at 1.5 $\mathrm{mW/cm^2}$, and then increased to 1050 nA at 3.0 $\mathrm{mW/cm^2}$. This phenomenon is usually explained by the ratio between the efficiency of photogeneration and the photon flux of absorption. The nonlinear relation of the variational photocurrent with light intensity can be fitted by the positive correlation $I_{\mathrm{ph}} \propto p^{\theta}$, and p is the irradiation intensity. The exponent θ represents the photocurrent response to the intensity of incident light. In the illustration in Fig. 5(b), θ is estimated to ∼0.92 under 360 nm light according to the fitted data. The slight deviation is caused by the complicated processes of carrier generation, recombination, and trapping in the n-SnO_2 MW/p-GaN heterojunction photodetector.

When operated under 360 nm ultraviolet illumination at −3 V bias, the responsivity (R) of the fabricated n-SnO_2 MW/p-GaN heterojunction photodetector reaches up to about 1.5 A/W [see Fig. 5(c)], while the corresponding detectivity (D^*) is extracted up to about 1.3×10^{13} Jones by varying the light intensity [see Fig. 5(d)]. The device parameters exhibit an excellent detection capability of the as-fabricated n-SnO_2 MW/p-GaN heterojunction photodetector. In addition, R and D^* decrease with an increase of light intensity, and these phenomena may be caused by the scattering and enhanced recombination of carriers.

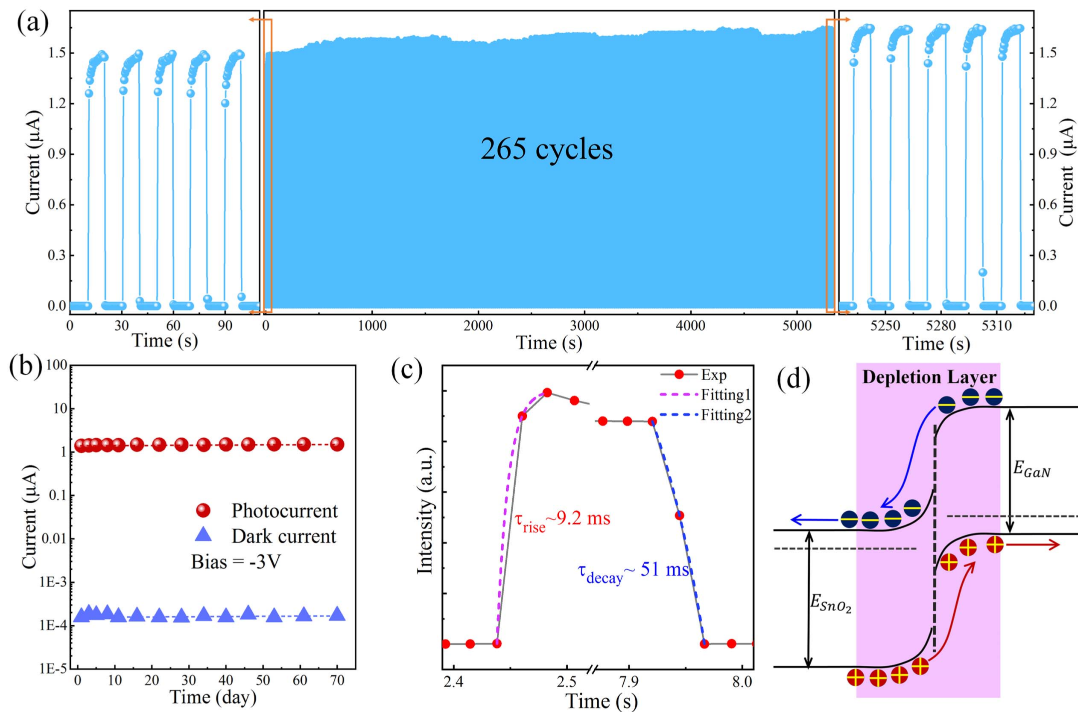

Fig. 6. (a) I-t curve of the fabricated n-SnO_2 MW/p-GaN heterojunction photodetector under 265 switching cycles of ultraviolet light illumination. (b) The variations of photocurrent and dark current when the photodetector was stored in the lab in ambient air for different time (~70 days). (c) Rise time and decay time of the n-SnO_2 MW/p-GaN heterojunction photodetector measured at the bias of −3 V. (d) Energy band diagram of the photodetector operated upon ultraviolet light irradiation. Under ultraviolet illumination, the generated electrons transport toward n-type SnO_2 MW on the conduction band, while the holes transport toward p-type GaN layer on the valence band.

The stability of the as-constructed n-SnO_2 MW/p-GaN heterojunction photodetector, one critical device parameter for their practical application, is checked. When operated at a reverse bias voltage of −3.0 V, the workable stability of the as-constructed n-SnO_2 MW/p-GaN photodetector was studied by utilizing 360 nm light at a light power intensity of 3.5 mW/cm^2. The switching performance via the I-t curve illustrated in Fig. 6(a) shows that the obtained photocurrent and dark current possessed negligible degradation in the whole measurement, indicating reliable light operation stability at the absence of encapsulation. In addition, the I_{light}/I_{dark} ratio is up to 10^4, as the dark current is measured to about 10^{-4} μA. After storing in lab in ambient air condition for about 70 days, the light current and dark current of the as-constructed photodetector were recorded at different times and are plotted in Fig. 6(b). Clearly, there is a weak fluctuation of currents, and a high I_{light}/I_{dark} ratio of nearly 10^4 was captured under the ultraviolet illumination via a 3.5 mW/cm^2 intensity even after storing in ambient air for 70 days, suggesting that the as-fabricated n-SnO_2 MW/p-GaN heterojunction photodetector exhibits quite good long-term storage stability without any encapsulation [7,25,54].

The investigation of the photoresponse was performed, and the quantificational research on the processes of this current rise and decay is represented by the time-dependent photocurrent curve, which is fitted by the exponential equation as follows [2,29,30,39]:

$$I = I_0 + Ae^{-t/\tau_1} + Be^{-t/\tau_2}. \quad (4)$$

In this equation, I_0 is the steady-state photocurrent, t is the time, A and B are fitting constants, and the fitting constant τ_1 is associated with the fast variation in the carrier concentration as the ultraviolet radiation is switched on/off. τ_2 is associated with carrier capture and release caused by intrinsic defects of the as-grown SnO_2 wires. The time constants of the rising and decaying edges are represented by τ_r and τ_d. Figure 6(c) displays the fitted results. The rising time (τ_r) and decaying time (τ_d) of the photodetector are obtained to be 9.2 and 51 ms, respectively. The obtained response times are faster than those of both p-GaN and SnO_2 MW-based photodetector devices, indicating that the constructed n-SnO_2 MW/p-GaN heterojunction can efficiently accelerate the separation of photogenerated carriers [42,59]. The research progress of SnO_2 nanowire/microwire-related photodetectors has been compared in recent years, and the response times of our fabricated n-SnO_2 MW/p-GaN photodetectors are also outstanding (see Table 1).

The working principle of the n-SnO_2 MW/p-GaN heterojunction device was exploited, and the energy band schematic diagram and photoelectric mechanism of the device under ultraviolet wave band illumination are shown in Fig. 6(d). As we described above, a built-in electric field could be formed toward the n-SnO_2/p-GaN interface, with the direction of the SnO_2 MW pointing to the p-GaN film [2,29,54]. When the device is

Table 1. Comparison between the Fabricated n-SnO_2 MW/p-GaN Heterojunction Photodetector in This Work and Other Previously Reported Works

Photodetector	Wavelength	Responsivity	Detectivity [Jones]	EQE	UV/vis Ratio	Response Time	Refs.
SnO_2 nanowire	320 nm	–	–	1.32×10^7%	–	–	[12]
SnO_2 film	290 nm	23 mA/W	–	10%	200	128/91 ms	[60]
SnO_2 microrod	260 nm	2×10^8 mA/W	–	1.5×10^7%	~10^4	<1/1 s	[41]
SnO_2 nanonets	320 nm	–	–	–	–	<50/50 s	[35]
SnO_2 nanowire arrays	370 nm	0.36 mA/W	3.02×10^9	–	1.8	0.72/1.78 s	[61]
ZnO – SnO_2 nanofibers	300 nm	–	–	–	–	32.2/7.8 s	[37]
SnO_2 MW/PEDOT:PSS	450 nm	0.018 mA/W	–	–	–	<2/2 s	[18]
SnO_2/CuZnS core-shell	300 nm	1.6 mA/W	5.41×10^{11}	0.63%	500	0.045/1.17 ms	[29]
SnO_2/GaN	360 nm	185 mA/W	2.81×10^{13}	74%	2.1×10^3	310 ns/61 μs	[2]
SnO_2 MW/$CsPbBr_3$	320 nm	1900 mA/W (3 V)	1.0×10^{13}	–	–	0.03/1.94 ms (0 V)	[30]
SnO_2 MW/GaN	360 nm	1450 mA/W	1.31×10^{13}	497%	1.5×10^3	9.2/51 ms	This work

exposed to irradiation of ultraviolet light, photogenerated carriers are produced, and then separated quickly by the external voltage. The photoelectrons and photoholes move to the In and Ni/Au electrodes, respectively. Thereby, the photocurrent is produced in the external circuit. The device can work as follows. (i) Due to Anderson's model and the carrier diffusion process, a built-in electric field is generated through balancing the drift motion and diffusion motion. (ii) Under the dark environment or radiation at an unresponsive wave band, the severe shortage of carriers inside the heterojunction and the depletion of charge diffused by carriers at the p-n interface can result in a higher barrier at the reverse biasing condition. (iii) Upon the ultraviolet radiation with the photon energy higher than 3.4 eV, a mass of nonequilibrium photoinduced carriers are generated in the depletion layer. With the increasing photocarriers concentration near the interface, the depletion region becomes wider and the intensity of the internal electric field increases. Driven by the external electric field, the photocarriers can be separated efficiently, thus prominently increasing the photocurrent. (iv) After the photogenerated carriers are separated, the electrons transport toward the n-SnO_2 MW on the conduction band and the holes transport toward the p-GaN layer on the valence band. Ultimately, the electrons and holes are collected by the In and Ni/Au electrodes, respectively, forming a loop current. Therefore, the as-constructed n-SnO_2 MW/p-GaN heterojunction device can enable both light emission and light detection using the same device structure. Both the LED and photodetector share an identical SnO_2/GaN heterointerface as the active region, and the device structure can be integrated into an individual chip to construct an on-chip photonic and optoelectronic circuit.

4. CONCLUSIONS

In conclusion, we demonstrate the realization of monolithically integrated ultraviolet LED and photodetector utilizing the same n-SnO_2 MW/p-GaN heterojunction. Owing to the radiative recombination of holes and electrons accumulating at the SnO_2/GaN heterointerface, the forward-biased LED exhibits uniform light emitting at 395.0 nm. Facilitated by its high sensitivity to the ultraviolet light, the photovoltaic-type ultraviolet photodetector based on the fabricated SnO_2/GaN heterojunction was also achieved, which exhibits an ultrahigh responsibility of 1.5 A/W and the rejection ratio of $R_{360\ nm}/R_{400\ nm} = 1.5 \times 10^3$. Moreover, the device has a high detectivity (1.3×10^{13} Jones) and a high photodark current ratio of 10^5 under the wavelength of 360 nm light at −3 V bias. The ultraviolet photodetecting character, especially for responsivity, is 1 order of magnitude larger than that of previously reported single SnO_2 microwire/nanowire-based ultraviolet photodetectors, and the rejection ratio is 2 orders of magnitude larger than the highest value ever reported for the one-dimensional wired p-n photodetectors. This work offers an effective way to obtain p-n heterojunction ultraviolet light-emitting/detecting optoelectronic devices, especially for the photodetection device, which have high responsivity, high rejection ratio, and low energy consumption.

Funding. Open Fund of Key Laboratory for Intelligent Nano Materials and Devices of the Ministry of Education (INMD-2020M03); Fundamental Research Funds for the Central Universities (NT2020019); National Natural Science Foundation of China (11774171, 11874220, 11974182, 21805137).

Disclosures. The authors declare no conflicts of interest.

REFERENCES

1. Y. Wu, Z. Li, K.-W. Ang, Y. Jia, Z. Shi, Z. Huang, W. Yu, X. Sun, X. Liu, and D. Li, "Monolithic integration of MoS_2-based visible detectors and GaN-based UV detectors," Photon. Res. **7**, 1127–1133 (2019).
2. L. Su, Y. Zuo, and J. Xie, "Scalable manufacture of vertical p-GaN/n-SnO_2 heterostructure for self-powered ultraviolet photodetector, solar cell and dual-color light emitting diode," InfoMat **3**, 598–610 (2021).
3. Q. Liu, Q. Xue, Y. Wang, X. Wei, and J. Hao, "Bifunctional device with high-energy storage density and ultralow current analog resistive switching," Adv. Electron. Mater. **7**, 2000902 (2021).
4. C. Han, C. Li, Z. Zang, M. Wang, K. Sun, X. Tang, and J. Du, "Tunable luminescent $CsPb_2Br_5$ nanoplatelets: applications in light-emitting diodes and photodetectors," Photon. Res. **5**, 473–480 (2017).
5. Q. Shan, C. Wei, Y. Jiang, J. Song, Y. Zou, L. Xu, T. Fang, T. Wang, Y. Dong, J. Liu, B. Han, F. Zhang, J. Chen, Y. Wang, and H. Zeng, "Perovskite light-emitting/detecting bifunctional fibres for wearable LiFi communication," Light Sci. Appl. **9**, 163 (2020).
6. J. Xie, P. Hang, H. Wang, S. Zhao, G. Li, Y. Fang, F. Liu, X. Guo, H. Zhu, X. Lu, X. Yu, C. C. S. Chan, K. S. Wong, D. Yang, J. Xu, and K. Yan, "Perovskite bifunctional device with improved electroluminescent and photovoltaic performance through interfacial energy-band engineering," Adv. Mater. **31**, 1902543 (2019).

7. W. Song, J. Chen, Z. Li, and X. Fang, "Self-powered MXene/GaN van der Waals heterojunction ultraviolet photodiodes with superhigh efficiency and stable current outputs," Adv. Mater. **33**, 2101059 (2021).
8. Q. Cai, H. You, H. Guo, J. Wang, B. Liu, Z. Xie, D. Chen, H. Lu, Y. Zheng, and R. Zhang, "Progress on AlGaN-based solar-blind ultraviolet photodetectors and focal plane arrays," Light: Sci. Appl. **10**, 94 (2021).
9. C. Wu, B. Du, W. Luo, Y. Liu, T. Li, D. Wang, X. Guo, H. Ting, Z. Fang, S. Wang, Z. Chen, Y. Chen, and L. Xiao, "Highly efficient and stable self-powered ultraviolet and deep-blue photodetector based on $Cs_2AgBiBr_6/SnO_2$ heterojunction," Adv. Opt. Mater. **6**, 1800811 (2018).
10. K. Liu, M. Sakurai, and M. Aono, "Controlling semiconducting and insulating states of SnO_2 reversibly by stress and voltage," ACS Nano **6**, 7209–7215 (2012).
11. M. Periyasamy and A. Kar, "Modulating the properties of SnO_2 nanocrystals: morphological effects on structural, photoluminescence, photocatalytic, electrochemical and gas sensing properties," J. Mater. Chem. C **8**, 4604–4635 (2020).
12. L. Hu, J. Yan, M. Liao, L. Wu, and X. Fang, "Ultrahigh external quantum efficiency from thin SnO_2 nanowire ultraviolet photodetectors," Small **7**, 1012–1017 (2011).
13. Y. Chen, W. Qiu, X. Wang, W. Liu, J. Wang, G. Dai, Y. Yuan, Y. Gao, and J. Sun, "Solar-blind SnO_2 nanowire photo-synapses for associative learning and coincidence detection," Nano Energy **62**, 393–400 (2019).
14. Y. Li, W. Yin, R. Deng, R. Chen, J. Chen, Q. Yan, B. Yao, H. Sun, S.-H. Wei, and T. Wu, "Realizing a SnO_2-based ultraviolet light-emitting diode via breaking the dipole-forbidden rule," NPG Asia Mater. **4**, e30 (2012).
15. S. Pan, W. Lu, Z. Chu, and G. Li, "Deep ultraviolet emission from water-soluble SnO_2 quantum dots grown via a facile 'top-down' strategy," J. Mater. Sci. Technol. **31**, 670–673 (2015).
16. X. Xue, L. Zhang, X. Geng, Y. Huang, B. Zhang, Y. Zhao, M. Xu, J. Yan, D. Zhang, and F. Zhao, "Effect of the aln interlayer on electroluminescent performance of n-SnO_2/p-GaN heterojunction light-emitting diodes," Mater. Sci. Semicond. Process. **91**, 409–413 (2019).
17. H. Zhou, R. Deng, Y.-F. Li, B. Yao, Z.-H. Ding, Q.-X. Wang, Y. Han, T. Wu, and L. Liu, "Wavelength-tuned light emission via modifying the band edge symmetry: doped SnO_2 as an example," J. Phys. Chem. C **118**, 6365–6371 (2014).
18. S. Li, S. Wang, K. Liu, N. Zhang, Z. Zhong, H. Long, and G. Fang, "Self-powered blue-sensitive photodetector based on PEDOT:PSS/SnO_2 microwires organic/inorganic p-n heterojunction," Appl. Phys. A **119**, 1561–1566 (2015).
19. A. D. Pramata, K. Suematsu, A. T. Quitain, M. Sasaki, and T. Kida, "Synthesis of highly luminescent SnO_2 nanocrystals: analysis of their defect-related photoluminescence using polyoxometalates as quenchers," Adv. Funct. Mater. **28**, 1704620 (2018).
20. N. Bhardwaj, B. Satpati, and S. Mohapatra, "Plasmon-enhanced photoluminescence from SnO_2 nanostructures decorated with Au nanoparticles," Appl. Surf. Sci. **504**, 144381 (2020).
21. C. Lin, Y. Lu, Y. Tian, C. Gao, M. Fan, X. Yang, L. Dong, and C. Shan, "Diamond based photodetectors for solar-blind communication," Opt. Express **27**, 29962–29971 (2019).
22. Z. Zhang, C. Lin, X. Yang, Y. Tian, C. Gao, K. Li, J. Zang, X. Yang, L. Dong, and C. Shan, "Solar-blind imaging based on 2-inch polycrystalline diamond photodetector linear array," Carbon **173**, 427–432 (2021).
23. S. Li, D. Guo, P. Li, X. Wang, Y. Wang, Z. Yan, Z. Liu, Y. Zhi, Y. Huang, Z. Wu, and W. Tang, "Ultrasensitive, superhigh signal-to-noise ratio, self-powered solar-blind photodetector based on n-Ga_2O_3/p-CuSCN core-shell microwire heterojunction," ACS Appl. Mater. Interfaces **11**, 35105–35114 (2019).
24. P. Wan, M. Jiang, T. Xu, Y. Liu, and C. Kan, "High-mobility induced high-performance self-powered ultraviolet photodetector based on single ZnO microwire/PEDOT:PSS heterojunction via slight Ga-doping," J. Mater. Sci. Technol. **93**, 33–40 (2021).
25. L. Su, W. Ouyang, and X. Fang, "Facile fabrication of heterostructure with p-BiOCl nanoflakes and n-ZnO thin film for UV photodetectors," J. Semicond. **42**, 052301 (2021).
26. C.-N. Lin, Y.-J. Lu, X. Yang, Y.-Z. Tian, C.-J. Gao, J.-L. Sun, L. Dong, F. Zhong, W.-D. Hu, and C.-X. Shan, "Diamond-based all-carbon photodetectors for solar-blind imaging," Adv. Opt. Mater. **6**, 1800068 (2018).
27. W. Dai, W. Liu, J. Yang, C. Xu, A. Alabastri, C. Liu, P. Nordlander, Z. Guan, and H. Xu, "Giant photothermoelectric effect in silicon nanoribbon photodetectors," Light Sci. Appl. **9**, 120 (2020).
28. M. Zervos, N. Lathiotakis, N. Kelaidis, A. Othonos, E. Tanasa, and E. Vasile, "Epitaxial highly ordered Sb:SnO_2 nanowires grown by the vapor liquid solid mechanism on m-, r- and a-Al_2O_3," Nanoscale Adv. **1**, 1980–1990 (2019).
29. J. Cai, X. Xu, L. Su, W. Yang, H. Chen, Y. Zhang, and X. Fang, "Self-powered n-SnO_2/p-CuZnS core-shell microwire UV photodetector with optimized performance," Adv. Opt. Mater. **6**, 1800213 (2018).
30. Y. Zhang, W. Xu, X. Xu, J. Cai, W. Yang, and X. Fang, "Self-powered dual-color UV-green photodetectors based on SnO_2 millimeter wire and microwires/$CsPbBr_3$ particle heterojunctions," J. Phys. Chem. Lett. **10**, 836–841 (2019).
31. L. Li, W. Gao, H. Chen, K. Zhao, P. Wen, Y. Yang, X. Wang, Z. Wei, N. Huo, and J. Li, "Strong anisotropy and piezo-phototronic effect in SnO_2 microwires," Adv. Electron. Mater. **6**, 1901441 (2020).
32. Z. Long, X. Xu, W. Yang, M. Hu, D. V. Shtansky, D. Golberg, and X. Fang, "Cross-bar SnO_2-NiO nanofiber-array-based transparent photodetectors with high detectivity," Adv. Electron. Mater. **6**, 1901048 (2020).
33. J. Yan, Y. Chen, X. Wang, Y. Fu, J. Wang, J. Sun, G. Dai, S. Tao, and Y. Gao, "High-performance solar-blind SnO_2 nanowire photodetectors assembled using optical tweezers," Nanoscale **11**, 2162–2169 (2019).
34. C.-H. Lin, R.-S. Chen, T.-T. Chen, H.-Y. Chen, Y.-F. Chen, K.-H. Chen, and L.-C. Chen, "High photocurrent gain in SnO_2 nanowires," Appl. Phys. Lett. **93**, 112115 (2008).
35. H. Chen, L. Hu, X. Fang, and L. Wu, "General fabrication of monolayer SnO_2 nanonets for high-performance ultraviolet photodetectors," Adv. Funct. Mater. **22**, 1229–1235 (2012).
36. Q.-M. Fu, J.-L. Peng, Z.-C. Yao, H.-Y. Zhao, Z.-B. Ma, H. Tao, Y.-F. Tu, Y. Tian, D. Zhou, and Y.-B. Han, "Highly sensitive ultraviolet photodetectors based on ZnO/SnO_2 core-shell nanorod arrays," Appl. Surf. Sci. **527**, 146923 (2020).
37. W. Tian, T. Zhai, C. Zhang, S.-L. Li, X. Wang, F. Liu, D. Liu, X. Cai, K. Tsukagoshi, D. Golberg, and Y. Bando, "Low-cost fully transparent ultraviolet photodetectors based on electrospun ZnO-SnO_2 heterojunction nanofibers," Adv. Mater. **25**, 4625–4630 (2013).
38. K. Liu, M. Sakurai, and M. Aono, "One-step fabrication of Ga_2O_3-amorphous-SnO_2 core-shell microribbons and their thermally switchable humidity sensing properties," J. Mater. Chem. **22**, 12882–12887 (2012).
39. J. Han, M. He, M. Yang, Q. Han, F. Wang, F. Zhong, M. Xu, Q. Li, H. Zhu, C. Shan, W. Hu, X. Chen, X. Wang, J. Gou, Z. Wu, and J. Wang, "Light-modulated vertical heterojunction phototransistors with distinct logical photocurrents," Light Sci. Appl. **9**, 167 (2020).
40. J. Zhao, R. Deng, J. Qin, J. Song, D. Jiang, B. Yao, and Y. Li, "Photoresponse enhancement in SnO_2-based ultraviolet photodetectors via coupling with surface plasmons of Ag particles," J. Alloy. Compd. **748**, 398–403 (2018).
41. K. Liu, M. Sakurai, M. Aono, and D. Shen, "Ultrahigh-gain single SnO_2 microrod photoconductor on flexible substrate with fast recovery speed," Adv. Funct. Mater. **25**, 3157–3163 (2015).
42. X. Xu, J. Chen, S. Cai, Z. Long, Y. Zhang, L. Su, S. He, C. Tang, P. Liu, H. Peng, and X. Fang, "A real-time wearable UV-radiation monitor based on a high-performance p-CuZnS/n-TiO_2 photodetector," Adv. Mater. **30**, 1803165 (2018).
43. H. Shi, B. Cheng, Q. Cai, X. Su, Y. Xiao, and S. Lei, "Surface state controlled ultrahigh selectivity and sensitivity for UV photodetectors based on individual SnO_2 nanowires," J. Mater. Chem. C **4**, 8399–8406 (2016).
44. H. Wu, Z. Su, F. Jin, H. Zhao, W. Li, and B. Chu, "Improved performance of perovskite photodetectors based on a solution-processed $CH_3NH_3PbI_3/SnO_2$ heterojunction," Org. Electron. **57**, 206–210 (2018).
45. X. Huang, Y.-Q. Yu, J. Xia, H. Fan, L. Wang, M.-G. Willinger, X.-P. Yang, Y. Jiang, T.-R. Zhang, and X.-M. Meng, "Ultraviolet

photodetectors with high photosensitivity based on type-II ZnS/SnO_2 core/shell heterostructured ribbons," Nanoscale **7**, 5311–5319 (2015).
46. L. Gan, M. Liao, H. Li, Y. Ma, and T. Zhai, "Geometry-induced high performance ultraviolet photodetectors in kinked SnO_2 nanowires," J. Mater. Chem. C **3**, 8300–8306 (2015).
47. C. Ling, T. Guo, W. Lu, Y. Xiong, L. Zhu, and Q. Xue, "Ultrahigh broadband photoresponse of SnO_2 nanoparticle thin film/SiO_2/p-Si heterojunction," Nanoscale **9**, 8848–8857 (2017).
48. C. Jia, Z. Lin, Y. Huang, and X. Duan, "Nanowire electronics: from nanoscale to macroscale," Chem. Rev. **119**, 9074–9135 (2019).
49. S. Chang, Y. Zhao, J. Tang, Z. Bai, L. Zhao, and H. Zhong, "Balanced carrier injection and charge separation of $CuInS_2$ quantum dots for bifunctional light-emitting and photodetection devices," J. Phys. Chem. C **124**, 6554–6561 (2020).
50. S. Shrivastava, T. Q. Trung, and N.-E. Lee, "Recent progress, challenges, and prospects of fully integrated mobile and wearable point-of-care testing systems for self-testing," Chem. Soc. Rev. **49**, 1812–1866 (2020).
51. M. Jiang, K. Tang, P. Wan, T. Xu, H. Xu, and C. Kan, "A single microwire near-infrared exciton-polariton light-emitting diode," Nanoscale **13**, 1663–1672 (2021).
52. M. Jiang, P. Wan, K. Tang, M. Liu, and C. Kan, "An electrically driven whispering gallery polariton microlaser," Nanoscale **13**, 5448–5459 (2021).
53. C. Kan, Y. Wu, J. Xu, P. Wan, and M. Jiang, "Plasmon-enhanced strong exciton-polariton coupling in single microwire-based heterojunction light-emitting diodes," Opt. Express **29**, 1023–1036 (2021).
54. L. Hu, J. Yan, M. Liao, H. Xiang, X. Gong, L. Zhang, and X. Fang, "An optimized ultraviolet-A light photodetector with wide-range photoresponse based on ZnS/ZnO biaxial nanobelt," Adv. Mater. **24**, 2305–2309 (2012).
55. L. Zhang, P. Wan, T. Xu, C. Kan, and M. Jiang, "Flexible ultraviolet photodetector based on single ZnO microwire/polyaniline heterojunctions," Opt. Express **29**, 19202–19213 (2021).
56. Y. Li, Z. Shi, W. Liang, L. Wang, S. Li, F. Zhang, Z. Ma, Y. Wang, Y. Tian, D. Wu, X. Li, Y. Zhang, C. Shan, and X. Fang, "Highly stable and spectrum-selective ultraviolet photodetectors based on lead-free copper-based perovskites," Mater. Horiz. **7**, 530–540 (2020).
57. Y. Zhang, S. Li, Z. Li, H. Liu, X. Liu, J. Chen, and X. Fang, "High-performance two-dimensional perovskite $Ca_2Nb_3O_{10}$ UV photodetectors," Nano Lett. **21**, 382–388 (2021).
58. D. Wang, X. Liu, S. Fang, C. Huang, Y. Kang, H. Yu, Z. Liu, H. Zhang, R. Long, Y. Xiong, Y. Lin, Y. Yue, B. Ge, T. K. Ng, B. S. Ooi, Z. Mi, J.-H. He, and H. Sun, "Pt/AlGaN nanoarchitecture: toward high responsivity, self-powered ultraviolet-sensitive photodetection," Nano Lett. **21**, 120–129 (2021).
59. C. Li, H. Wang, F. Wang, T. Li, and L. Shen, "Ultrafast and broadband photodetectors based on a perovskite/organic bulk heterojunction for large-dynamic-range imaging," Light Sci. Appl. **9**, 31 (2020).
60. T. Oshima, T. Okuno, and S. Fujita, "UV-B sensor based on a SnO_2 thin film," Jpn. J. Appl. Phys. **48**, 120207 (2009).
61. P. Chetri and J. C. Dhar, "Self-powered UV detection using SnO_2 nanowire arrays with Au Schottky contact," Mater. Sci. Semicond. Process. **100**, 123–129 (2019).